Available online at www.sciencedirect.com
ScienceDirect
Journal of Sound and Vibration 325 (2009) 471–488
JOURNAL OF SOUND AND VIBRATION
www.elsevier.com/locate/jsvi

Order-crossing removal in Gabor order tracking by independent component analysis

Yu Guo[a,*], Kok Kiong Tan[b]

[a]*Faculty of Mechanical and Electrical Engineering, Kunming University of Science and Technology, Kunming 650093, PR China*
[b]*Department of Electrical and Computer Engineering, National University of Singapore, Singapore 117576, Singapore*

Received 14 January 2008; received in revised form 2 March 2009; accepted 4 March 2009
Handling Editor: J. Lam
Available online 8 April 2009

Abstract

Order-crossing problems in Gabor order tracking (GOT) of rotating machinery often occur when noise due to power–frequency interference, local structure resonance, etc., is prominent in applications. They can render the analysis results and the waveform-reconstruction tasks in GOT inaccurate or even meaningless. An approach is proposed in this paper to address the order-crossing problem by independent component analysis (ICA). With the approach, accurate order analysis results can be obtained and the waveforms of the order components of interest can be reconstructed or extracted from the recorded noisy data series. In addition, the ambiguities (permutation and scaling) of ICA results are also solved with the approach. The approach is amenable to applications in condition monitoring and fault diagnosis of rotating machinery. The evaluation of the approach is presented in detail based on simulations and an experiment on a rotor test rig. The results obtained using the proposed approach are compared with those obtained using the standard GOT. The comparison shows that the presented approach is more effective to solve order-crossing problems in GOT.

1. Introduction

Order tracking (OT) [1–10] plays an important role in the condition monitoring and fault diagnosis of rotating machinery. Differing from conventional vibration signal processing methods which are mainly applied to the constant speed operation modes of rotating machinery, OT aims to monitor the varying speed modes of rotating machinery, especially during the periods of start-up or shut-down, when the signals to be monitored do not meet the stationarity requirements of the *discrete Fourier transform* (DFT). In general, OT techniques can be classified into two categories [1,2]: waveform *reconstruction* and *non-reconstruction*. The Gabor OT (GOT) [1–4] and the Vold–Kalman filtering OT (VKFOT) [5–9] are two popular waveform reconstruction OT schemes which can extract or reconstruct the time domain waveforms of specific order components from the recorded signals. It is worth mentioning that research works [5] have shown that the GOT scheme is superior to the VKFOT scheme in waveform reconstruction. GOT carries out the time domain

*Corresponding author. Tel.: +86 871 5170917 4101; fax: +86 871 5194243.
E-mail address: kmgary@163.com (Y. Guo).

0022-460X/$ - see front matter © 2009 Elsevier Ltd. All rights reserved.
doi:10.1016/j.jsv.2009.03.003

waveform reconstruction of specific order components by applying Gabor expansion (see Eq. (1)) to the corresponding Gabor coefficients. This process is also called a time-varying filtering process [11]. However, as in most signal processing applications, the noise present will distort the results. If there exists order-crossing noise caused by power–frequency interferences, local structure resonances, etc., the Gabor coefficients near the crossing points will be affected by both the order components of interest and the unwanted crossing noise. As a result, the extracted waveforms are distorted when using these noise-infiltrated Gabor coefficients near the crossing points. Recently, some researchers have proposed a method to solve the order-crossing problem via an improved GOT scheme [1,2]. However, it requires a pre-requisite that a specific spectral/order component has a smooth amplitude variation and a continuous phase change.

Recently, the method known as independent component analysis (ICA) [12–23] has evoked intense attentions with its promising applications to separate observed mixed signals into different independent components (ICs)[1] with different statistical properties [12–18]. Currently, ICA has been applied to feature extraction in linguistic data analysis [19], image recognition [20] and mechanical fault detection [21–23]. However, some properties of ICA [19], including the permutation and the scaling ambiguities restrain the ICA from wider engineering applications.

In this paper, we propose an approach to remove the order-crossing noise in GOT by combining the GOT scheme with the ICA. Here, ICA is exploited to extract the signal of interest which can contain multiple-order components, e.g., $1\times, 2\times, 3\times$, order components from the mixed vibration with order-crossing disturbances, and GOT is employed to reconstruct the waveform of a specific order component from the extracted signal. The approach has the advantage that the pre-requisite required for solving order-crossing problem in GOT will be removed. In addition, the permutation ambiguity and scaling ambiguity of the ICA are solved in our scheme to enable the approach to be amenable to practical applications. Brief reviews of the GOT and the ICA will be introduced in Section 2. Our approach is presented in Section 3. The approach to solve the ambiguities is introduced in Section 4. Subsequently, results from a simulation and an experiment on a rotor test rig are shown in Section 5. Finally, conclusions are drawn in Section 6.

2. Review of GOT and ICA

2.1. Gabor order tracking (GOT)

The GOT is a novel OT scheme proposed by Qian et al. [3–5], which takes advantage of Gabor transform, being one of the invertible linear joint time–frequency transforms, to get an insight into the time-varying behaviors of the analyzed signal, and it allows waveform reconstruction of specific order components via the corresponding inverse transform. In this subsection, we will give a brief introduction to the theory of the GOT.

2.1.1. Gabor transform pair

The Gabor transform pair is composed of the Gabor transform and the inverse Gabor transform or Gabor expansion. The Gabor expansion is first proposed by Gabor [24]. For a signal $s(t)$, the Gabor expansion is defined by

$$s(t) = \sum_{m=-\infty}^{\infty} \sum_{n=-\infty}^{\infty} c_{m,n} h_{m,n}(t), \tag{1}$$

where $c_{m,n}$ is named as the Gabor coefficient and $h_{m,n}(t)$ is called the Gabor elementary function given by

$$h_{m,n}(t) = h(t - mT)\, e^{jn\Omega t}, \quad m, n = 0, \pm 1, \pm 2, \ldots, \tag{2}$$

[1]It is worth noting that the term 'component' is used in ICA and other signal processing techniques, such as time–frequency analysis (TFA) and OT with different meanings. In ICA, the 'component' is related and traced back to an independent signal source. In many other signal processing techniques, 'component' refers to a frequency component of a signal. So, if a signal has two frequencies, there are two frequency components in it. For example, assuming a mixed signal is composed of a square wave and a triangular wave. If the square wave and the triangle wave are generated from different signal sources, each of them is an IC of the mixed observed signal according to the principles of ICA (assuming they are non-Gaussian and mutually independent). But each one of them is a multi-component signal as far as frequency components are concerned, the way component is used in TFA, OT, etc.

where T and Ω denote the time and frequency sampling steps, respectively. Although $h(t)$ can be of other forms than a Gaussian function [25], traditionally, the set of $h_{m,n}(t)$ functions are expressed as the time- and frequency-shifted versions of the Gaussian function $h(t)$ which is defined by

$$h(t) = \left(\frac{\alpha}{\pi}\right)^{1/4} \mathrm{e}^{-(\alpha/2)t^2}, \tag{3}$$

where α is an adjustable parameter and it can be exploited to strike a balance between the time and the frequency resolutions of $h(t)$ according to applications. It is worth mentioning that the calculation of the Gabor coefficient $c_{m,n}$ has remained unsolved for a long time since the Gabor expansion was presented over half a century ago. In the 1980s, Bastiaans [26] discovered the relationship between the *short Fourier transform* (STFT) and the Gabor coefficient. The Gabor coefficient can be calculated by

$$c_{m,n} = STFT[mT, n\Omega] = \int_{-\infty}^{\infty} s(t)\gamma^*_{m,n}(t)\,\mathrm{e}^{-\mathrm{j}n\Omega t}\,\mathrm{d}t, \tag{4}$$

which is the sampled STFT and it is also known as the Gabor transform, where

$$\gamma_{m,n}(t) = \gamma(t - mT)\,\mathrm{e}^{\mathrm{j}n\Omega t}, \quad m, n = 0, \pm 1, \pm 2, \ldots \tag{5}$$

is the time- and frequency-shifted versions of $\gamma(t)$ (the dual function of $h(t)$) and the asterisk * denotes a complex conjugate. The relationship between $h(t)$ and $\gamma(t)$ is expressed by

$$\sum_{m=-\infty}^{\infty} \sum_{n=-\infty}^{\infty} h_{m,n}\gamma^*_{m,n}(\tau) = \delta(t - \tau), \tag{6}$$

where $\delta(t)$ denotes the Dirac δ function. Eqs. (1) and (4) form the Gabor transform pair. It is worth mentioning that usually there does not exist an analytical solution to $\gamma(t)$ for a given $h(t)$ but a numerical solution [11].

2.1.2. GOT procedures

One of the most interesting applications of the Gabor expansion is in time-varying filtering and it is exploited in GOT to carry out the waveforms reconstruction of specific order components. The main steps of GOT in the context of condition monitoring and fault diagnosis of rotating machinery are shown in Fig. 1 and it can be briefly described as follows [27]:

- *Step* 1: *Data acquisition*. Synchronously acquire the tachometer channel and the vibration channel at a constant sample rate. Thereafter, the tachometer data series $p[k]$ and vibration data series $s[k]$ are available.

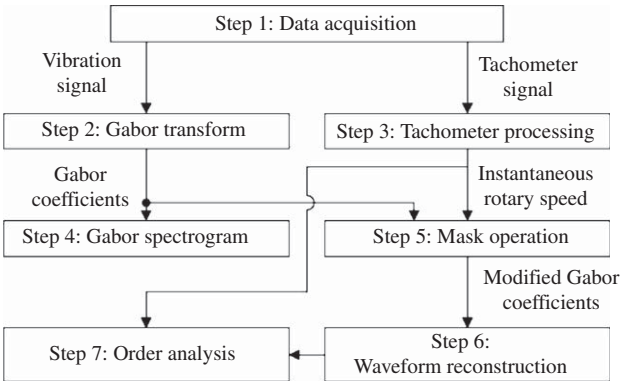

Fig. 1. Flowchart of GOT procedure.

- *Step* 2: *Gabor transform*. Obtain the initial Gabor coefficient array $c_{m,n}$ by a discrete version of Gabor transform in Eq. (4), which is given in Refs. [3,27] as

$$c_{m,n} = \sum_{k=0}^{L-1} \tilde{s}[k]\gamma^*[k - m\Delta M]\, e^{-j2\pi nk/N}, \quad 0 \leqslant m < M, \ 0 \leqslant n < N, \tag{7}$$

where ΔM represents the time sampling interval, N and M denote the total number of frequency bins and time points, respectively. Hence, the total number of Gabor coefficients $c_{m,n}$ is equal to MN. $\tilde{s}[k]$ denotes a periodic extension of sampling series $s[k]$ given in Refs. [3,27] as

$$\tilde{s}[k + iL] = \begin{cases} s[k], & 0 \leqslant k < L_s, \\ 0, & L_s \leqslant k < L, \end{cases} \quad i = \pm 1, \pm 2, \ldots, \tag{8}$$

where L denotes the period of data series $\tilde{s}[k]$ and L_s represents the length of the data series $s[k]$. Note that L is the smallest integer that is bigger than or equal to L_s, and it must be exactly divisible by the time sampling interval ΔM and the total number of frequency bins N, viz. $M = L/\Delta M$ and $N = L/\Delta N$, where ΔN represents the frequency sampling interval.

- *Step* 3: *Gabor spectrogram*. Mapping the Gabor coefficient array $c_{m,n}$ into a 2D image, the Gabor spectrogram is generated. The Gabor spectrogram is composed of an $M \times N$ time–frequency lattices (the Gabor time–frequency lattices). The intensity of each lattice in the image represents the amplitude of $c_{m,n}$ at a particular time bin m and a particular frequency bin n.
- *Step* 4: *Tachometer processing*. Calculate the angular speed $\omega(t)$ from tachometer signal with $\omega(t_i) = d\theta(t_i)/dt|_{t=t_i}$, where t_i denotes the arrival time corresponding to the cumulative rotation angle $\theta(t_i)$. $\omega(t_i)$ is determined by the tachometer used in applications. For example, if the tachometer provides one pulse per revolution, then $\theta(t_i) = 2\pi \times i$, $i = 0, 1, 2, \ldots$, where i denotes the ith tachometer pulses. In applications, t_i is determined by a specified trigger level to the tachometer series $p[k]$. For example, if 5 (V) is selected as the trigger level, we can consider t_i as the time instant when $p[k]$ first crosses 5 (V) in one pulse of tachometer signal. A digital differentiator is exploited to obtain a more accurate rotational speed (see Ref. [27] for more detail). Furthermore, the rotary speed RPM is calculated by $RPM = \omega(t)/2\pi \times 60$ *revolution per minute* (rev/min).
- *Step* 5: *Mask operation*. A mask operation is performed on the initial Gabor coefficient array $c_{m,n}$ by the rotary speed RPM and a specified order $l\times$. First, we locate the position index of the $l\times$ component on Gabor time–frequency lattices according to [27]

$$index = round\left(\frac{RPM}{60} \times \frac{N}{f_s} \times l\right), \tag{9}$$

where N is the number of frequency bins of the Gabor time–frequency lattices, f_s denotes the sampling frequency and *round* represents the round-off operation. Subsequently, a mask array $w_{m,n}$ is generated with limited binary values, 1 or 0, whose size is the same as the Gabor coefficient array $c_{m,n}$. It behaves as a mask,

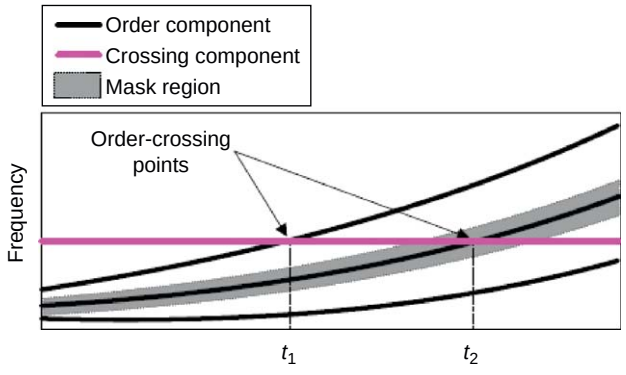

Fig. 2. Example of the crossing problem shown in time–frequency spectrogram.

preserving $c_{m,n}$ when $w_{m,n}=1$ and removing $c_{m,n}$ when $w_{m,n}=0$. The coefficients corresponding to $w_{m,n}=1$ make up the mask region (see Fig. 2), which is determined by the boundaries $l\times RPM/60\pm\Delta f/2$, where Δf is a adjustable frequency bandwidth. Δf can be set to be a constant value, such as 5 Hz, or a constant order bandwidth, such as $r\times RPM/60$ (see Ref. [27] for more detail). Finally, a modified Gabor coefficient array $\tilde{c}_{m,n}$ is generated by

$$\tilde{c}_{m,n}=\begin{cases} c_{m,n}, & w_{m,n}=1,\\ 0, & w_{m,n}=0. \end{cases} \tag{10}$$

- *Step* 6: *Waveform reconstruction.* Reconstruct the time history of the specified order $l/$ from the modified coefficient array $\tilde{c}_{m,n}$ by performing the discrete version of Gabor expansion in Eq. (1), which is given in Refs. [3,27] as

$$s_l[k]=\sum_{m=0}^{M-1}\sum_{n=0}^{N-1}\tilde{c}_{m,n}h[k-m\,\Delta M]\,\mathrm{e}^{\mathrm{j}2\pi nk/N}, \tag{11}$$

where $s_l[k]$ denotes the reconstructed data series of the $l\times$ component. It is worth mentioning that the ratio $Q=N/\Delta M$ is defined as the Gabor sampling ratio. For $Q=1$, we have critical sampling and we have oversampling when $Q>1$ and undersampling when $Q<1$. In general, $Q\geqslant 1$ is needed for a reliable waveform reconstruction.

- *Step* 7: *Order analysis.* Calculate the waveform magnitude and phase of selected order components as a function of the speed.

2.1.3. Order-crossing problems in GOT

The Gabor transform pair enables GOT to be used as a powerful tool for condition monitoring and fault diagnosis during varying speed operations of rotating machinery. However, the waveform reconstruction by mask operations can be distorted at t_1 and t_2, respectively (see Fig. 2, where the Gabor coefficients are distorted by order-crossing noise at the crossing points).

Recently, Pan et al. [1,2] proposed a scheme to solve the order-crossing problem in GOT. It exploits a 'Canny' operation, which is an image-processing algorithm, to modify the Gabor coefficients which are affected by the crossing components. The kernel ideal is based on the assumption that a specific order component will have smoothly varying amplitude and continuously changing phase, and the phenomena exists even during occurrences of order crossing [1,2]. In this paper, an approach which is independent of these assumptions to remove order-crossing noise in GOT based on ICA is presented, and a new way to solve this problem is attempted.

2.2. Independent component analysis (ICA)

Recently, ICA has evoked intense attentions with its promising applications to separate a mixture of signal sources into different sources or ICs according to the their statistical properties. The main initial ideas can be briefly expressed by the following mixed model

$$\begin{pmatrix} x_1\\ x_2\\ \vdots\\ x_m \end{pmatrix}=\begin{pmatrix} a_{11} & a_{12} & \cdots & a_{1n}\\ a_{21} & a_{22} & \cdots & a_{2n}\\ \cdots & \cdots & \cdots & \cdots\\ a_{m1} & a_{m2} & \cdots & a_{mn} \end{pmatrix}\begin{pmatrix} s_1\\ s_2\\ \vdots\\ s_n \end{pmatrix}, \tag{12}$$

which can in turn be formulated into a vector–matrix notation,

$$\mathbf{x}=\mathbf{A}\mathbf{s}, \tag{13}$$

where the m-dimensional column vector $\mathbf{x}$, contains elements which are observed or recorded mixed signals; $\mathbf{A}$ is the $m\times n$ mixing matrix, and its element a_{ji} is decided by the transfer path between a source and a sensor; the n-dimensional column vector $\mathbf{s}$ represents different independent sources, i.e., ICs. In our study, the mixing

matrix, **A**, is square ($m = n$) or complete. If the number of ICs is less than the dimensions of the observed vectors, $m > n$, the task is deemed to be undercomplete. In standard ICA formulations, the matrix **A** is restricted to $m \geqslant n$. If $m < n$, the task becomes overcomplete, but it is still solvable [28]. In Eq. (12) or (13), the column vector **x** can be obtained from measurements by different kinds of sensors according to the signals' natures in applications. For example, microphones are adopted in speech, and acoustics and eddy sensors are suitable for displacement measurements which are employed in our tests. Making the column vector **s** the subject,

$$\mathbf{s} = \mathbf{W}\mathbf{x}, \tag{14}$$

where **W**, the separating matrix, is the inverse of matrix **A** and it can be expressed by $\mathbf{W} = \mathbf{A}^{-1}$. **A** is unknown, so a solution for **s** does not seem to exist. However, according to the principle of ICA, it is possible to estimate the transfer matrix **A** based on the statistical properties of the element s_i in the column vector **s**. Once **A** is obtained, the column vector **s** can be solved.

ICA aims to obtain the separating matrix, **W**, and then the column vector **s**. It is worth pointing out that ICA includes linear ICA and nonlinear ICA in general. However, in our study, we focus on the linear ICA only. The linear ICA is profused with a rich number of approaches and algorithms. It is also model independent with the data for analysis, and only the non-Gaussianity probability density functions of the ICs of analyzed data are required. It functions as an unique feature to most practical applications such as vibration analysis. FastICA [13–16] is a popular linear ICA algorithm due to the required computation being highly efficient, robust and amenable to applications. We will use it for signals separation in our study. The approach to obtain **W** in ICA is to measure the non-Gaussianity. Kurtosis and negentropy can be exploited to measure the non-Gaussianity which are also called contrast functions. However, in applications, kurtosis can be very sensitive to outliers and negentropy is difficult to be computed [18]. So, in the FastICA algorithm, approximations of negentropy is a compromise to both kurtosis and negentropy. The computation steps will be briefly presented in our approach with the test data series.

3. Scheme for order-crossing noises removal in GOT

As mentioned in Section 2, GOT plays an important role in condition monitoring and fault diagnosis of rotating machinery. However, in applications, the order-crossing problem can distort the Gabor coefficients near the crossing points which will in turn affect the waveform reconstruction of specific order components and results of OT. On the other hand, the ICA has the ability to separate mixed signals into ICs. In theory, the order components and the crossing components arise from different sources and they are different in their inherent statistical properties. Hence, if the two techniques are used together, a new way to segregate the order components from the crossing component mixed signals can be formulated. The results verify positively our scheme and support the new approach to remove order-crossing noise in GOT. It is worth mentioning that we will test our approach with the mixed signals which contain three and two different ICs in the simulation experiment and test experiment, respectively. One IC is related to the order components, and others are related to the order-crossing components. In applications, one IC corresponds to the order components in the mixed signals. It is clear that the order components arise from one vibration source, the monitored rotor, and they are related to the rotating speed. The rest of the mixed signals can be considered to be the non-order noise which is independent of the rotating speed. However, the non-order noise may not be caused by only one source. It is possible that the non-order noise comes from multiple sources. According to the principle of ICA, our scheme can be extended to remain viable when there are more disturbance signals by exploiting multiple sensors to ensure the number of vibration sensors is not less than the number of independent sources of vibration (required by FastICA scheme). The schematic of our approach is shown in Fig. 3.

The main steps can be described as follows:

- *Step* 1: *Multi-channel data sampling.* Synchronously acquire the tacho channel and vibration channels at a constant sampling rate. Vibration channels are composed of m vibration sensors measuring vibrations at different positions, and yielding observed mixed signals $(x_1(t), x_2(t), \ldots, x_m(t))$ for ICA (m is set as 3 and 2 in the simulation and experimental study, respectively). The tacho pulses are acquired from tacho channel for calculating the rotating speed in GOT.

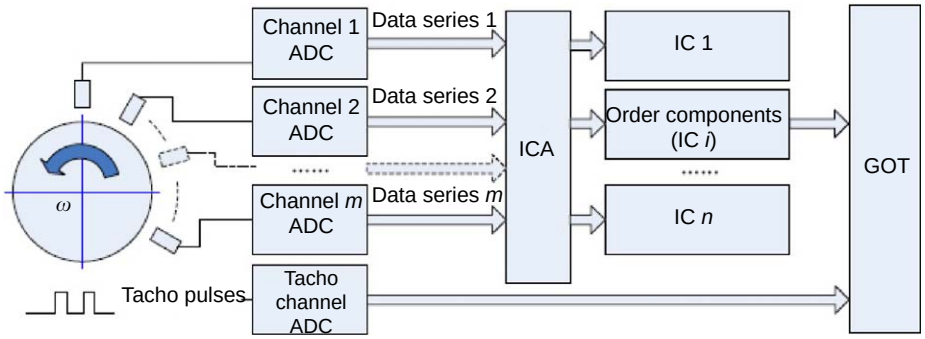

Fig. 3. Schematic of order-crossing noise removal in GOT.

- *Step* 2: *Mixed signals separation by ICA.* Before executing the FastICA algorithm, there are some preprocessing steps for ICA which should be performed [15]. First, *centering*, which will remove the means of the observed mixed signals $(x_1(t), x_2(t), \ldots, x_m(t))$ and make the column vector $\mathbf{x}$ zero-mean. Subsequently, *sphering* or *whitening* is applied to the observed vector $\mathbf{x}$ directly. It is a linear transformation of $\mathbf{x}$ to a new vector $\mathbf{y}$ in which all elements are uncorrelated with unity variances, viz. $E\{\mathbf{y}\mathbf{y}^{\mathrm{T}}\} = \mathbf{I}$ where E denotes expectation. $\mathbf{y}$ is calculated via $\mathbf{y} = \mathbf{E}\mathbf{D}^{-1/2}\mathbf{E}^{\mathrm{T}}\mathbf{x}$ where $\mathbf{E}$ denotes the orthogonal matrix of eigenvectors of $E\{\mathbf{x}\mathbf{x}^{\mathrm{T}}\}$ and $\mathbf{D}$ is the diagonal matrix of its eigenvalues [13,15]. Approximations of negentropy is presented by *Hyväinen* for measuring non-Gaussianity in the FastICA algorithms, which can be expressed by

$$J(y_i) \approx c[E\{G(y_i)\} - E\{G(\upsilon)\}]^2, \tag{15}$$

where G is practically any non-quadratic function and its choice is discussed in Ref. [13], c is a constant, and υ is a Gaussian variable of zero mean and unit variance. E denotes expectation, which in practice would be estimated by sample mean over y_i. Based on a fixed-point iteration scheme [13,15] for finding one IC as $y_i = \mathbf{w}^{\mathrm{T}}\mathbf{x}$ by maximizing the function $J_G(\mathbf{w})$

$$J_G(\mathbf{w}) = [E\{G(\mathbf{w}^{\mathrm{T}}\mathbf{x})\} - E\{G(\upsilon)\}]^2, \tag{16}$$

where w is an n-dimensional vector constrained so that $E\{(\mathbf{w}^{\mathrm{T}}\mathbf{x})^2\} = 1$. A deflation scheme [13] is exploited to estimate the other ICs systematically, and then Eq. (16) is extended to obtain the whole matrix $\mathbf{W}$ in Eq. (14), which is expressed in Ref. [13] as

$$\max \sum_{i=1}^{n} J_G(\mathbf{w}_i) \quad \text{wrt. } i = 1, \ldots, n. \tag{17}$$

As a result, n ICs are obtained through Eqs. (17) and (14) (n is derived as 3 and 2 in the simulation and experimental study, respectively); one IC is pertaining to the order components and others are pertaining to the order-crossing noise components.

- *Step* 3: *GOT.* Apply GOT to the separated order components for OT analysis.

Here, the ambiguities of ICA should be addressed. First, the permutation ambiguity in ICA, which means we cannot determine the order of the separated ICs. Hence, a question arises over the order components we are interested in. Second, the scaling ambiguity in ICA, which means we cannot determine the amplitudes (energies) of the ICs. Two schemes will be presented to solve these two problems in Section 4.

4. Solutions to ambiguities of ICA in GOT

4.1. Solution to permutation problem

In OT, order components refer to the components which vary with the rotation speed. On the contrary, the order-crossing components are independent of the rotation speed. Hence, in our approach, we employ the

linear correlation coefficients or *Pearson product-moment correlation coefficients* (PMCCs) between each separated IC and the rotation speed as a criterion (in application, the absolute value of PMCC is used) to determine which IC represents the order components automatically. The formula of PMCC is given by

$$\rho_{xy} = \frac{cov(xy)}{\sigma_x \sigma_y} = \frac{E(xy) - E(x)E(y)}{\sqrt{E(x^2) - E^2(x)}\sqrt{E(y^2) - E^2(y)}}, \tag{18}$$

where E is the expected value operator, *cov* means covariance, and x and y are two random variables with standard deviations σ_x and σ_y. According to statistics, the correlation coefficient ρ_{xy} is always in the interval $[-1, 1]$. If two measured variables have a linear relation, ρ_{xy} is close to 1 (positive correlation) or -1 (negative correlation) and if there is no linear relation between the two variables, ρ_{xy} is close to zero. Although the relationship between the order component related IC and the tacho signal is not a linear relation, its inherent relationship with the rotating speed makes the corresponding correlation coefficient (absolute value) larger than that coming from the non-order components and the tacho signal. If an order-crossing problem is caused by two sets of order components, the two sets of order components should be related to two different rotational speeds. For example, in Ref. [7] (see p. 1144) 'Synthetic signal 2: Two sets of reference revolution speeds are designated, where one is the same as that used in synthetic signal 1, and the other speeds up from stationary to 9000 rev/min during 2 and 5 s.' The approach proposed in our paper is employed to remove the order-crossing problem for one set of order components resulting from the other sets of order components or other disturbances. Except the one set of order components related to the rotation speed, the other sets are independent of the rotation speed and they are referred to as 'the order-crossing components' in our paper. Subsequently, the OT can be only applied to the separated IC of order components. Simulations and tests will justify the effectiveness of the scheme in solving the permutation problem of ICA in GOT.

4.2. Solution to scaling problem

In some applications such as speech and image processing, the scaling ambiguity from ICA is not a problem. But in condition monitoring and fault diagnosis of machinery, this can become a problem when we compare with past results. In our scheme, a method to solve the problem by an iterative algorithm is developed. It calculates the attenuation factor (AF) for re-scaling by the *least sum square* (LSS) method. It can be expressed by

$$\min D(\alpha) = \sum_{n=0}^{N-1} (\alpha y_n - \hat{y}_n)^2, \tag{19}$$

where D denotes the distance of two variables, α represents the adjustable AF and y_n is a part of the amplitude plot of a specific order component (e.g., $1\times$) by GOT, which is from a part of observed signal without order-crossing problem. For example, the GOT result of a part of a specific order component is not close to t_1 and t_2 in Fig. 1. It can be chosen to avoid the interference of order-crossing points by means of time–frequency spectrogram. $\hat{y}_n$ is the corresponding OT result of the specific order component from ICA. Here, it represents an amplified predicted value with a high *signal-noise ratio* (SNR) after the separation by ICA. In the algorithm, we wish to find the AF, α, such that the two results fit best according to the defined error criterion of Eq. (19).

5. Experiments

5.1. Simulation

The proposed approach is applied to a simulation model for evaluating the accuracy of numerical solution by our approach. The main steps of the simulation are as follows:

- *Step* 1: *Modeling.* A second-order linear system is modeled and used to emulate the mechanical system of rotating machinery with a *natural frequency* $\omega_n = 2\pi \times 100$ rad/s and a *damping ratio* $\zeta = 1/4\pi \approx 0.08$.

The *frequency response function* (FRF) of the simulation system is given by

$$H(\mathrm{j}\omega) = \frac{100,000}{(\mathrm{j}\omega)^2 + 100\mathrm{j}\omega + 394,784}. \tag{20}$$

- *Step* 2: *Vibration emulation.* To emulate the start-up operation mode, we define a multi-order vibration source measured at three positions by

$$s_p(t) = A_p[\sin\theta_p(t) + \sin 3\theta_p(t) + \sin 5\theta_p(t)], \quad p = 1,2,3, \tag{21}$$

where the suffixes p denotes different mounted positions of sensors and it is also used in following equations. In the simulation, $A_1 = 1$, $A_2 = 0.9$, $A_3 = 0.7$; $\theta_1(t) = 2\pi f(t)t$ with $f(t) = 0.5t^2$, $\theta_2(t) = \theta_1(t + t_{d1})$ and $\theta_3(t) = \theta_1(t + t_{d2})$. Symbol t_d denotes a time delay between the sensors as determined by the propagation speed and path of the vibration. $t_{d1} = 0.00003$ s and $t_{d2} = -0.00001$ s, relative to the first source. It is worth mentioning that FastICA is based on an instantaneous mixing model which means that if the time delay between sensors is zero, the best separation effect can be achieved. In a practical application, if sensors are mounted closely, the time delay between sensors can be kept small and negligible, since the vibration rapidly propagates through metal. Furthermore, different vibration sources incur different time delays in general, since the vibration propagation paths are different. According to the definition of instantaneous frequency [29],

$$f_i(t) = \frac{1}{2\pi}\frac{\mathrm{d}\varphi(t)}{\mathrm{d}t}, \tag{22}$$

and by substituting $\varphi(t) = \theta_1(t)$ to Eq. (22), we obtain the *instantaneous frequency* $f_i(t) = 1.5t^2$ for the first source in the simulation (the suffix i denotes *instantaneous*). Subsequently, by setting the time t, in the time interval $(2, 10)$, $f_i(t)$ is changed form 6 to 150 Hz and the corresponding rotation speed, rev/min, $n_i(t) = 60 \times f_i(t)$ will change from 360 to 9000 rev/min (the speed range is selected from 1060 to 8760 rev/min in the following GOT results).

- *Step* 3: *Emulating two order-crossing disturbance signals.* In our study, we emulate a start-up running condition where there are two different disturbance sources existing at the same time. First, we emulate a non-coherent start-up order-crossing disturbance signal which is composed of three harmonics and given by the following equations:

$$d_{1p}(t) = B_p(t)[\sin\alpha_p(t) + \sin 2\alpha_p(t) + \sin 3\alpha_p(t)], \quad p = 1,2,3, \tag{23}$$

where $B_p(t)$ represents a time-varying amplitude at position p, i.e., $B_1(t) = t/10$, $B_2(t) = 0.9B_1(t)$ and $B_3(t) = 0.7B_1(t)$; $\alpha_1(t) = 2\pi f(t)t + 0.1$ and $f(t) = 5t$, $\alpha_2(t) = \alpha_1(t + t_{d3})$ and $\alpha_3(t) = \alpha_1(t + t_{d4})$. For the second source, the time-delay parameters are set as $t_{d3} = 0.00005$ s and $t_{d4} = 0.00003$ s in the simulation. Second, we define another strong order-crossing signal with a constant frequency 50 Hz to simulate a local resonance or power–frequency disturbance signal. The disturbance signal is given by

$$d_{2p}(t) = C_p \sin\beta_p(t), \tag{24}$$

where C_p represents a amplitude at position p, i.e., $C_1 = 1$, $C_2 = 0.9$ and $C_3 = 0.95$; $\beta_1(t) = 2\pi f_0 t + 0.2$ and $f_0 = 50$ Hz, $\beta_2(t) = \beta_1(t + t_{d5})$ and $\beta_3(t) = \beta_1(t + t_{d6})$. For the third source, the time-delay parameters used are $t_{d5} = 0.000025$ s and $t_{d6} = -0.000025$ s.

- *Step* 4: *Emulating the mixed observed signals for ICA.* Let the vibration signals be convolved with the *impulse response function* (IRF) of the simulation system. The zero-noise signals at three positions are calculated by

$$z_p(t) = s_p(t) * h(t), \quad p = 1,2,3, \tag{25}$$

where $z_p(t)$ $(p = 1,2,3)$ represents three zero-noise signals, respectively, $*$ denotes convolution, $h(t) = \mathrm{IFT}[H(\mathrm{j}\omega)]$ is the IRF of the simulation system, here IFT denotes *inverse Fourier transform*. Subsequently, adding the order-crossing disturbance signals to $z_p(t)$ $(p = 1,2,3)$, respectively, we have

$$\tilde{z}_p(t) = z_p(t) + d_{1p}(t) + d_{2p}(t), \quad p = 1,2,3, \tag{26}$$

where $\tilde{z}_p(t)$ $(p = 1, 2, 3)$ denotes three mixed signals, respectively. Finally, acquiring the mixed signals at a constant sampling ratio 10,000 Hz, the mixed observed signals for ICA are generated.

5.2. Simulated GOT results based on ICA

In this section, we will show the GOT results from three categories of signals, which include the signals with zero-noise, the signals with order-crossing disturbances and the signals with order-crossing disturbances separated with ICA. Observations will be drawn from the results comparing signals from the three categories.

The time domain waveforms of the emulated signals at position 1 are shown in Fig. 4; the time domain waveforms of the mixed signal at the different positions are shown in Fig. 5 and the time domain waveforms of ICs obtained from the mixed signals following ICA separation are shown in Fig. 6.

By comparing the time domain waveforms shown in Figs. 4–6, it is easy to see that the disturbance in Fig. 5 is almost removed by ICA. In Fig. 6, the sequence and the amplitude are different from that shown in Fig. 4 due to the mentioned ambiguities of ICA. The time–frequency spectrograms of the mixed signal at position 1 and the separated ICs based on Gabor transform with a Gaussian window (1024 points, $\alpha = 2.5$, see Eq. (3)) are shown in Fig. 7.

In Fig. 7(a), the order-crossing problem caused by the two disturbance signals is clearly visible. On the contrary, in Fig. 7(b)–(d), the ICs relating to different sources are well separated by ICA separation and the order-crossing disturbance can hardly be noticed (the scaling ambiguity of ICA is visible; amplitude is expressed linearly with 64 gray levels).

The permutation-ambiguity solution mentioned in Section 4.1 is employed to ICs and as a result, the IC of interest is selected automatically and it will be processed as the signal with order-crossing disturbances separated with ICA at the subsequent steps. Subsequently, applying GOT to the three categories of signals, respectively, the corresponding amplitudes and phases are shown in Figs. 8 and 9. We find that the amplitudes and phases of the $1\times$ and the $3\times$ components are significant distorted by the order-crossing problem in Figs. 8b and 9b.

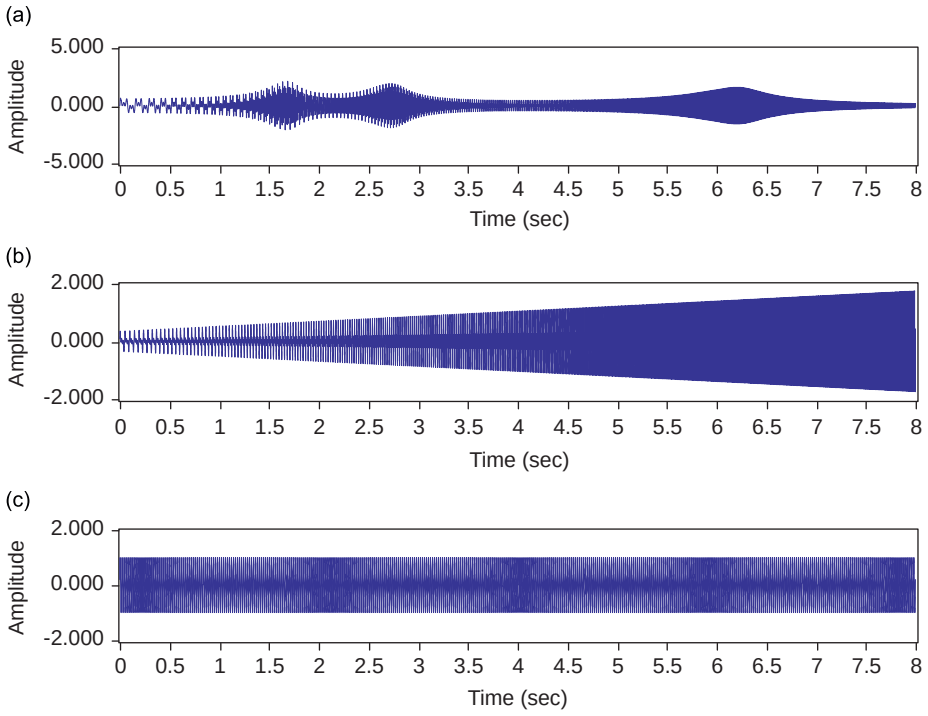

Fig. 4. Time domain waveforms of emulated signals at position 1: (a) $s_x(t)$; (b) $d_{1x}(t)$ and (c) $d_{2x}(t)$.

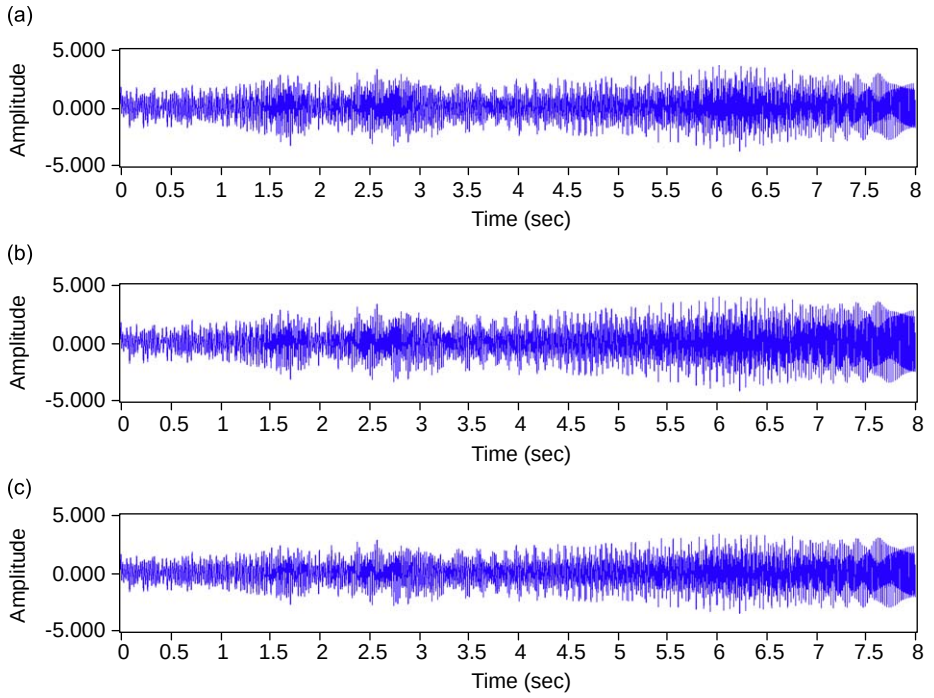

Fig. 5. Time domain waveforms of mixed signals: (a) mixed signal at position 1; (b) mixed signal at position 2 and (c) mixed signal at position 3.

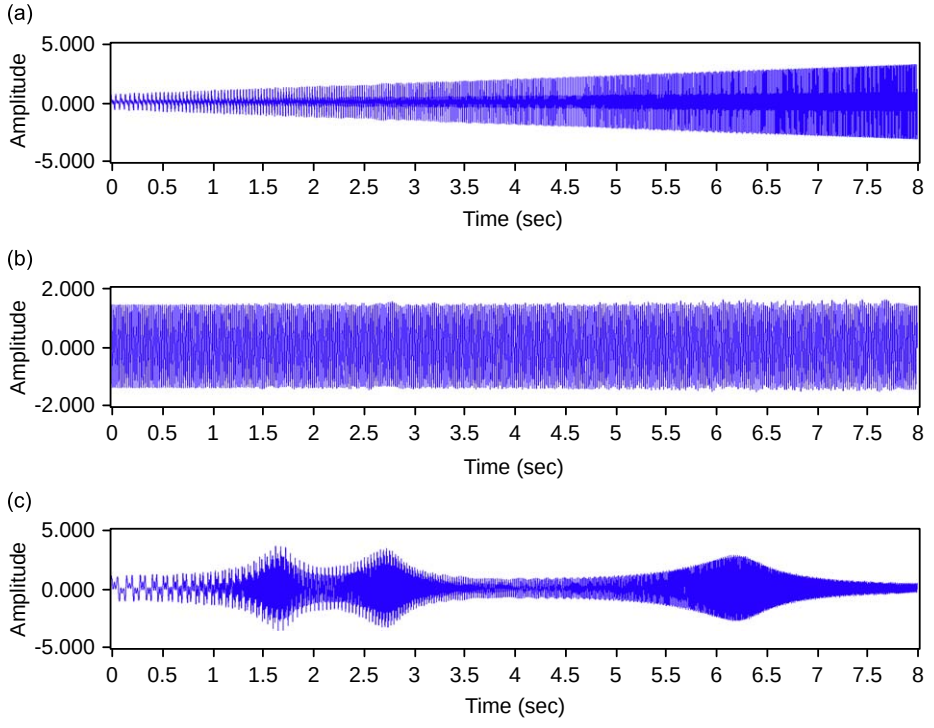

Fig. 6. Time domain waveforms of ICs obtained by a ICA separation: (a) IC 1; (b) IC 2 and (c) IC 3.

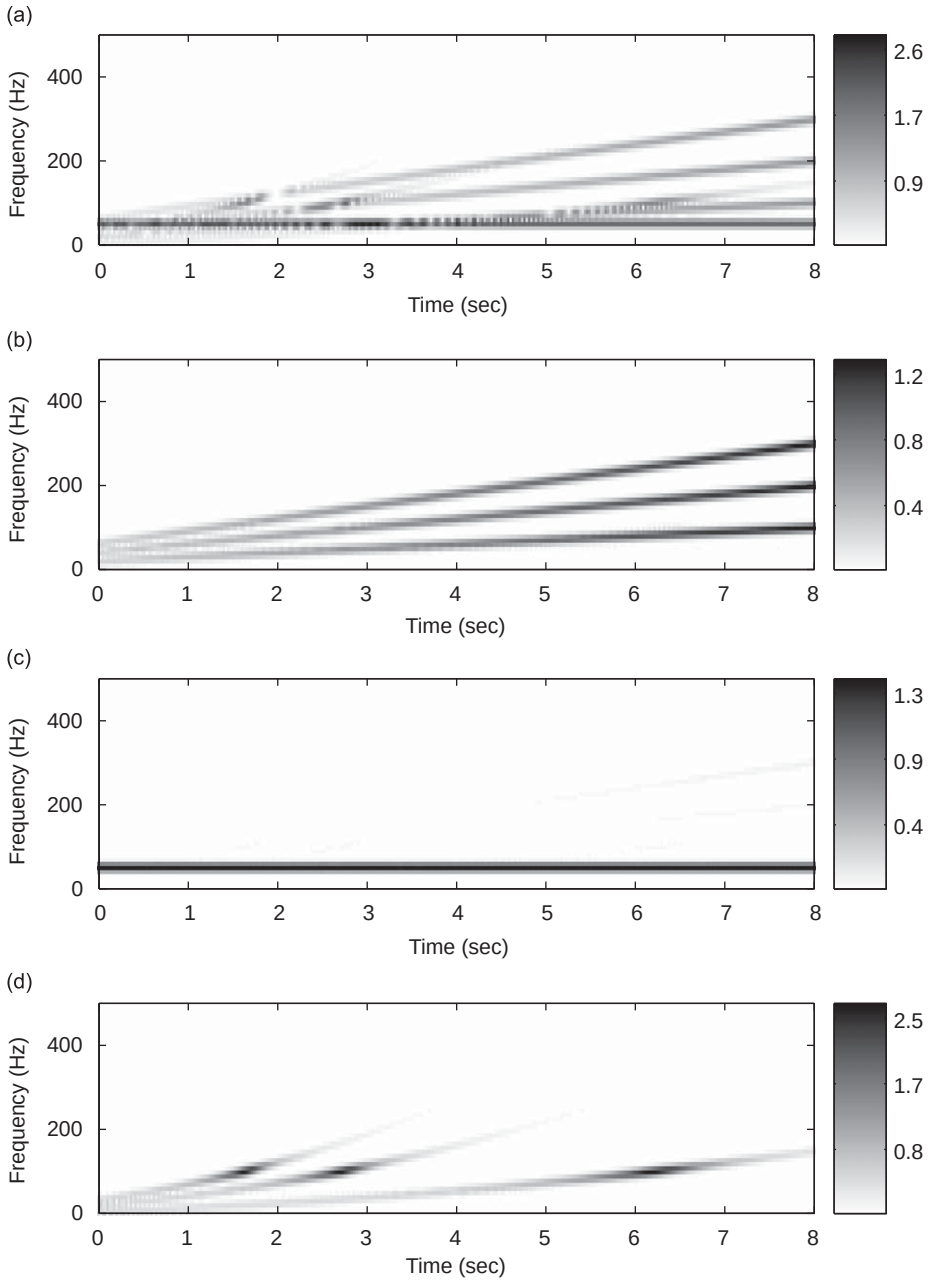

Fig. 7. Time–frequency spectrograms of mixed signal at position 1 and ICs obtained by ICA separation: (a) the mixed signal; (b) IC 1; (c) IC 2 and (d) IC 3.

In Fig. 8(c), the *natural frequency* of 100 Hz of the simulation system is clearly evident from both the $1\times$ and the $3\times$ components corresponding to the rotating speed at 6000 rev/min) ($1\times$) and 2000 rev/min ($3\times$).[2] Compared with Fig. 8(a) (the true value), the forms of the curves are very similar though the amplitudes are different. In Fig. 9(c), the phase variation of the signal is also clearly evident and it is almost the same as

[2]OT can be employed to track a spectral component like a resonance. However, we did not claim the ICA can be used to track resonance in OT. The ICA is used to remove the order-crossing disturbance before GOT is used to track a spectral component in the proposed approach.

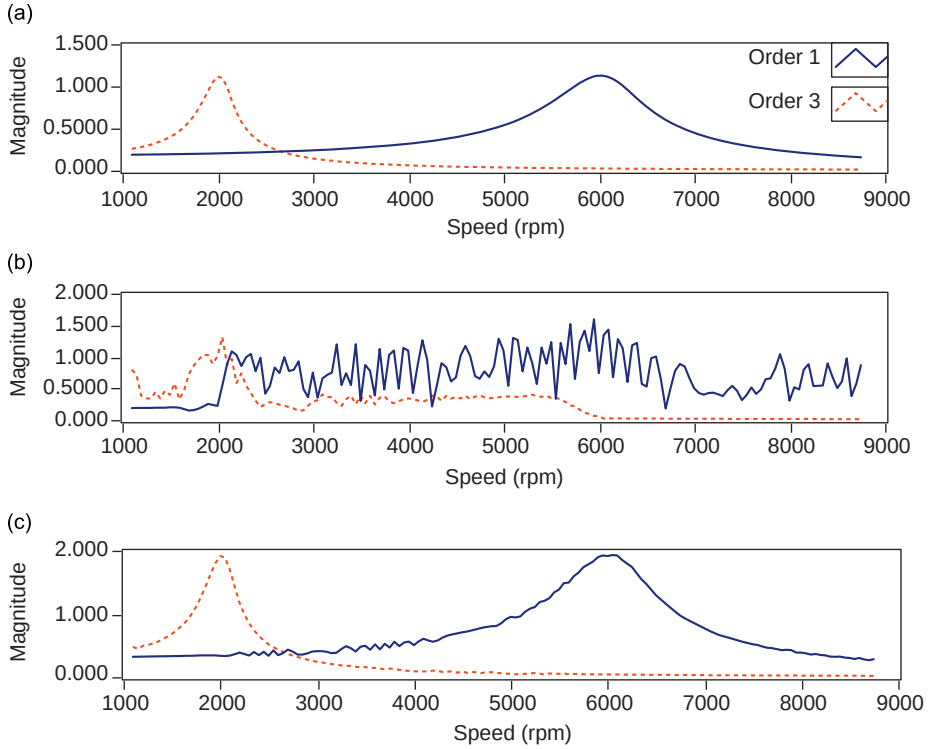

Fig. 8. Amplitudes of 1×, 3× component by using GOT to (emulated signal): (a) the signal with zero-noise; (b) the signal mixed with order-crossing noise and (c) the signal mixed with order-crossing noise following ICA separation.

the true phase variation shown in Fig. 9(a). It is worth mentioning that a phase change of 180° may be possible since the *whitening* step of ICA will cause the vector $\mathbf{y}$ to have a unit variance, $E\{\mathbf{y}\mathbf{y}^{\mathrm{T}}\} = \mathbf{I}$ (see the step 2 in Section 3). The sign of each element y_i still remains: one could multiply an element by -1 without affecting the model [19].

The results of the waveform reconstruction of the 1× order component from the mixed signal at position 1 and the interested IC are shown in Fig. 10. It is another clear evidence to support the proposed scheme in the paper.

The scaling ambiguity exist in all above results following ICA separation. To solve the problem, the re-scaling scheme mentioned in Section 4.2 is exploited. First, a part of the result is selected as y_n (see Eq. (19)) from the GOT results in Fig. 8. For example, in our simulation, we choose the amplitude of 1× order component at the speed range from 1100 to 1600 rev/min. Subsequently, applying our re-scaling scheme to obtain the AF α by Eq. (19), the re-scaled amplitude plot is shown in Fig. 11. Compared with the result from the zero-noise signal (true value) in Fig. 11, there is little difference. It is worth mentioning that FastICA scheme allows the mixed signals to contain one highly super-Gaussian IC [13]. This is a novel property of the proposed approach for applications.

5.3. Test

A test on a rotor test rig is also described here to demonstrate the practical applicability of the presented approach. Some information about the test is first given: the test rig is shown in Fig. 12. The rotor is driven by a DC motor which can rotate at a speed proportional to its input voltage. In the test, the input maximal voltage is about 110 V and the corresponding rotating speed is about 11,000 rev/min. Two eddy probes were mounted to obtain the horizontal vibration and vertical vibration signals, respectively, and the calibration sensitivities are 3.723 V/mm (horizontal) and 4.132 V/mm (vertical), respectively, with a maximum linear range of 2 mm and frequency range of 0–8 kHz. It is worth pointing out that the mounting positions of vibration

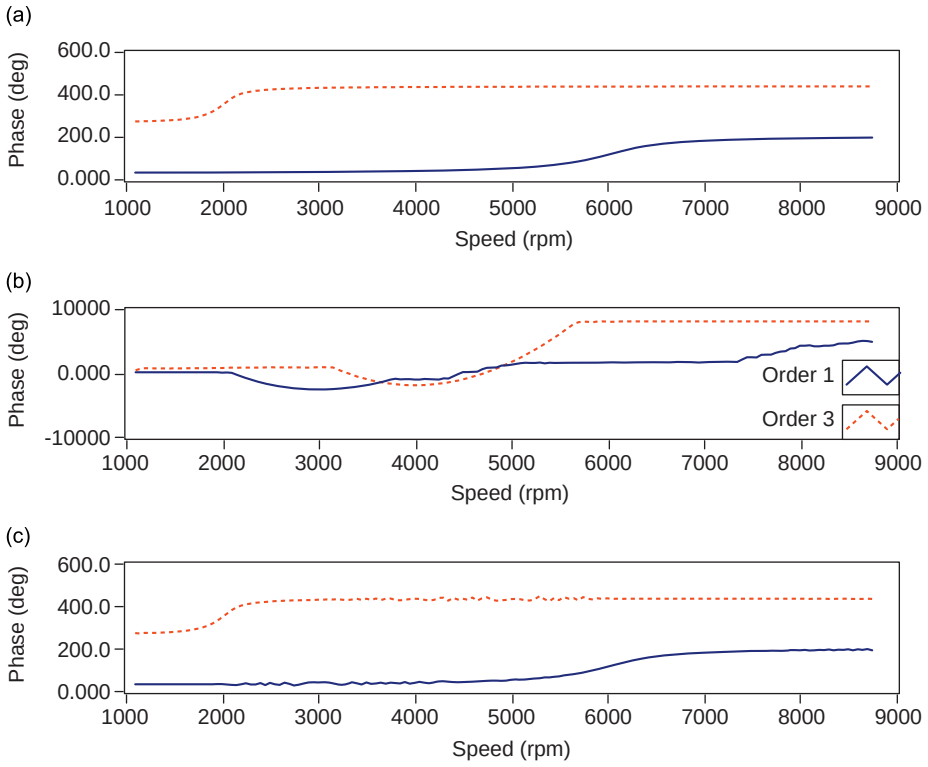

Fig. 9. Phases of $1\times$, $3\times$ component by applying GOT to (emulated signal): (a) the signal with zero-noise; (b) the signal mixed with order-crossing noise and (c) the signal mixed with order-crossing noise following ICA separation.

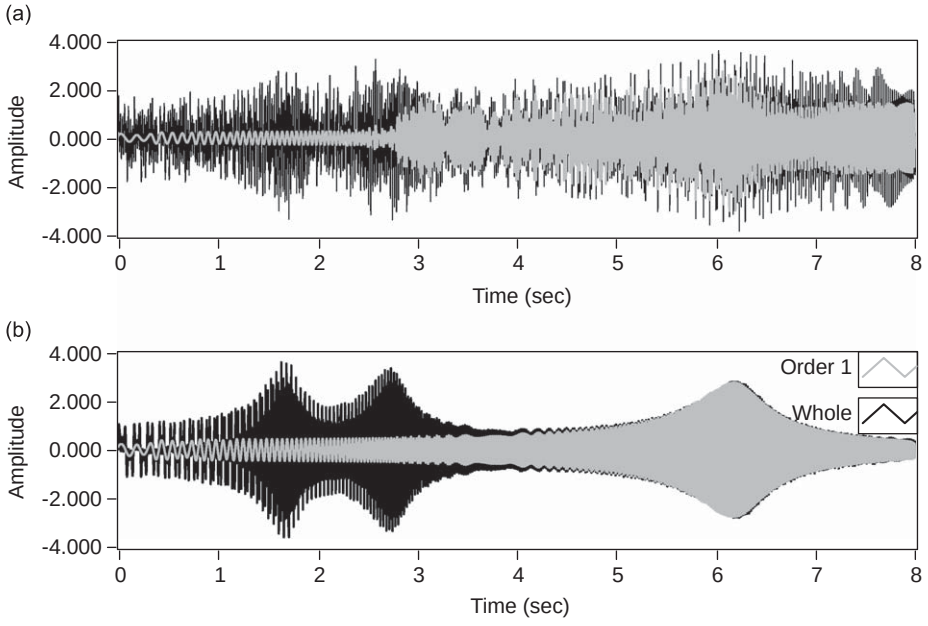

Fig. 10. Time domain waveform extracted by GOT from (emulated signal): (a) the signal mixed with order-crossing noise and (b) the signal mixed with order-crossing noise following ICA separation.

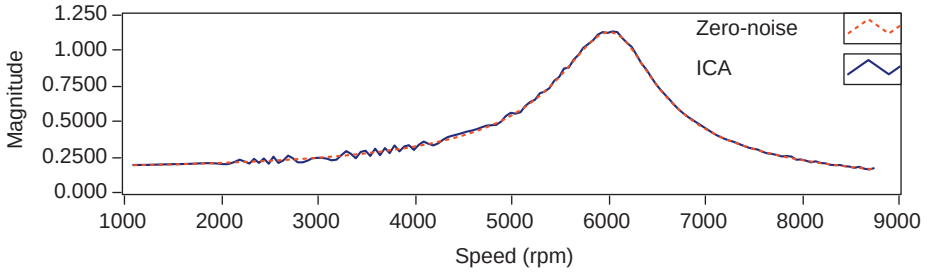

Fig. 11. Amplitude of 1× component in the IC of interest following with re-scaling scheme ($AF = 1.70967$, D = 9.6144E − 5) (compared with that of zero-noise signal at position 1).

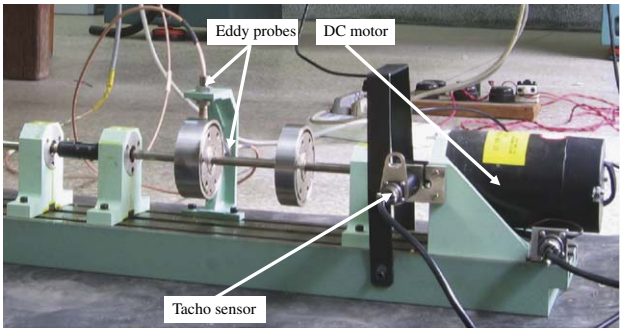

Fig. 12. Test rig.

sensors are not fixed, and any mounting position can be chosen where convenient for vibration pickup. A tacho sensor was also mounted, which will output tacho pulses. NI USB-9233A was used to sample the three analog inputs synchronously with a constant sampling rate: 20,000 Hz during the rotor's shut-down. Since the order-crossing noise in the original signals is not notable, and for a vivid show of the proposed approach, a deliberately introduced disturbance signal with a fundamental frequency of 50 Hz and its two harmonics (100 and 150 Hz) is added to simulate a power–frequency interference. The disturbance signal is given by

$$d_p(t) = A_p[\sin\psi_p(t) + 0.7\sin 2\psi_p(t) + 0.5\sin 3\psi_p(t)], \quad p = 1, 2, \tag{27}$$

where the suffix $p = 1$ and 2 denote horizontal position and vertical position, respectively; $A_1 = 1$, $A_2 = 0.8$; $\psi_1(t) = 2\pi f_0 t$ and $f_0 = 50$ Hz; $\psi_2(t) = \psi_1(t + t_{d7})$, where $t_{d7} = 0.00005$ s.

The time–frequency spectrograms of the original vibration data series at horizontal position, the order-crossing disturbance mixed data series and the separated ICs based on Gabor transform are shown in Fig. 13 (a down-sampling ratio 40 is applied for showing the 1× component of the original vibration data series).

In Fig. 13(b), it can be found that the order-crossing disturbance is much stronger than the original vibration. The spectrograms of separated ICs by the presented approach are, respectively, shown in Fig. 13(c) and (d). It is clear that the order-crossing disturbance is almost removed and the order components of interesting is well separated (see Fig. 13(d)).

Fig. 14 shows the amplitude of GOT to the order-crossing disturbance augmented signal, the original signal and the ICA separated signal with re-scaling, respectively. We find that the results obtained with ICA separated signal is much better compared to those obtained from the signal with the order-crossing noise. There are also differences in the results between the original signal and the ICA separated signal. One reason for the difference is that the original signals through eddy probes by ADC include the background noise. Another reason for the difference is that there is little difference in the FRF of the two eddy probes used in the test. However, it clearly discloses the resonance frequency (about 4600 rev/min or 76.67 Hz) and the order amplitude variation with the rotating speed of tested system, which is very useful for the condition monitoring and diagnosis of rotating machinery.

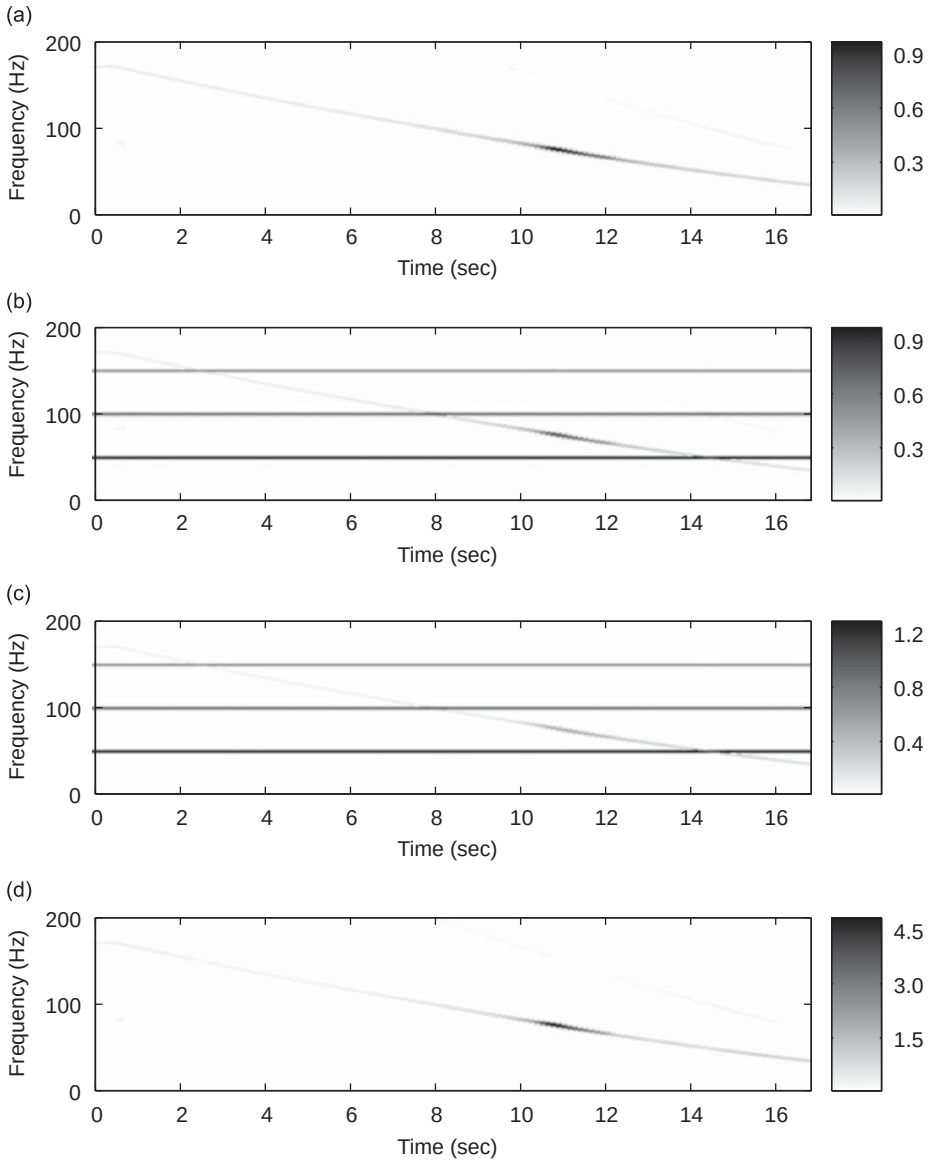

Fig. 13. Time–frequency spectrograms of mixed signal at horizontal position and ICs obtained by ICA separation: (a) original acquired signal; (b) order-crossing disturbance mixed signal; (c) IC 1 and (d) IC 2.

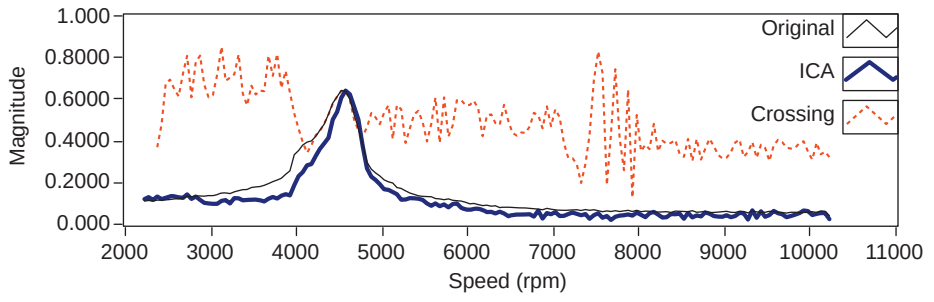

Fig. 14. Amplitude of 1× component after applying GOT to three categories of test data (for ICA re-scaled result: $AF = 4.40667$, $D = 0.00437966$).

All the algorithms in our study have been coded in Matlab and LabVIEW (include NI Sound and Vibration Measurement Suite).

6. Conclusions

This paper proposed a new approach to remove order-crossing disturbance in GOT. In the approach, the ICA scheme is employed to separate order components from recorded signals distorted by order-crossing noise and it is independent of prior assumptions made in the literature. The ambiguities of ICA are also solved in the approach which make it amenable to engineering applications. The theoretical and implementation details of the approach clearly show that the proposed ICA-GOT scheme provides a viable way to solving order-crossing problems in GOT.

References

[1] M.C. Pan, C.C. Chiu, Investigation on improved Gabor order tracking technique and its applications, *Journal of Sound and Vibration* 295 (3–5) (2006) 810–826.
[2] M.C. Pan, S.W. Liao, C.C. Chiu, Improvement on Gabor order tracking and objective comparison with Vold–Kalman filtering order tracking, *Mechanical Systems and Signal Processing* 21 (2) (2007) 653–667.
[3] S. Qian, Gabor expansion for order tracking, *Sound and Vibration* 37 (6) (2003) 18–22.
[4] H. Shao, W. Jin, S. Qian, Order tracking by discrete Gabor expansion, *IEEE Transactions on Instrumentation and Measurement* 52 (3) (2003) 754–761.
[5] M.F. Albright, S. Qian, A comparison of the newly proposed Gabor order tracking technique vs. other order tracking methods, SAE Paper No. 2001-01-1471, 2001.
[6] H. Vold, M. Mains, J. Blough, Theoretical foundation for high performance order tracking with the Vold–Kalman tracking filter, SAE Paper No. 972007, 1997.
[7] M.C. Pan, Y.F. Lin, Further exploration of Vold–Kalman-filtering order tracking with shaft-speed information—I: theoretical part, numerical implementation and parameter investigations, *Mechanical Systems and Signal Processing* 20 (5) (2006) 1134–1154.
[8] M.C. Pan, Y.F. Lin, Further exploration of Vold–Kalman-filtering order tracking with shaft-speed information—II: engineering applications, *Mechanical Systems and Signal Processing* 20 (6) (2006) 1410–1428.
[9] M.C. Pan, Adaptive Vold–Kalman filtering order tracking, *Mechanical Systems and Signal Processing* 21 (8) (2007) 2957–2969.
[10] M. Bai, J. Huang, M. Hong, F. Su, Fault diagnosis of rotating machinery using an intelligent order tracking system, *Journal of Sound and Vibration* 280 (3–5) (2005) 699–718.
[11] S. Qian, D. Chen, Joint time–frequency analysis, *IEEE Signal Processing Magazine* 16 (2) (1999) 53–67.
[12] P. Comon, Independent component analysis a new concept?, *Signal Processing* 36 (3) (1994) 287–314.
[13] A. Hyvärinen, Fast and robust fixed-point algorithms for independent component analysis, *IEEE Transactions on Neural Networks* 10 (3) (1999) 626–634.
[14] A. Hyvärinen, E. Oja, A fast fixed-point algorithm for independent component analysis, *Neural Computation* 9 (7) (1997) 1483–1492.
[15] A. Hyvärinen, E. Oja, Independent component analysis: algorithms and applications, *Neural Networks* 13 (2000) 411C43.
[16] A. Hyvärinen, A family of fixed-point algorithms for independent component analysis, *Proceedings of IEEE International Conference on Acoustics, Speech and Signal Processing* (*ICASSP*'97), Munich, Germany, 1997, pp. 3917–3920.
[17] A. Hyvärinen, Complexity pursuit: separating interesting components from time-series, *Neural Computation* 13 (4) (2001) 883–898.
[18] A. Hyvärinen, A unifying model for blind separation of independent sources, *Signal Processing* 85 (2005) 1419–1427.
[19] T. Honkela, A. Hyvärinen, Linguistic feature extraction using independent component analysis, *Proceedings of IEEE International Joint Conference on Neural Networks*, Vol. 1, Budapest, Hungary, 2004, pp. 279–284.
[20] J. Kim, J. Choi, J. Yi, M. Turk, Effective representation using ICA for face recognition robust to local distortion and partial occlusion, *IEEE Transactions on Pattern Analysis and Machine Intelligence* 27 (12) (2005) 1977–1981.
[21] M.J. Roan, J.G. Erling, L.H. Sibul, A new, non-linear, adaptive, blind source separation approach to gear tooth failure detection and analysis, *Mechanical Systems and Signal Processing* 16 (5) (2002) 719–740.
[22] S. Addisson, V. Luis, I. Jorge, G. Jorge, Blind source separation for classification and detection of flaws in impact-echo testing, *Mechanical Systems and Signal Processing* 19 (6) (2005) 1312–1325.
[23] Z. Li, Y. He, F. Chu, J. Han, W. Hao, Fault recognition method for speed-up and speed-down process of rotating machinery based on independent component analysis and factorial hidden Markov model, *Journal of Sound and Vibration* 291 (1–2) (2006) 60–71.
[24] D. Gabor, Theory of communication, *Journal of the Institute of Electrical Engineers* 93 (111) (1946) 429–457.
[25] S. Qian, D. Chen, Optimal biorthogonal analysis window function for discrete Gabor transform, *IEEE Transactions on Signal Processing* 42 (3) (1994) 694–697.
[26] M.J. Bastiaans, On the sliding-window representation in digital signal processing, *IEEE Transactions on Acoustics, Speech, and Signal Processing* 33 (4) (1985) 868–873.

[27] *Order Tracking Toolset User Manual*, National Instruments Corporation, 2003.
[28] T.W. Lee, M.S. Lewicki, M. Girolami, T.J. Sejnowski, Blind source separation of more sources than mixtures using overcomplete representations, *IEEE Signal Processing Letters* 6 (4) (1999) 87–90.
[29] B. Boashash, Interpreting and estimating the instantaneous frequency of a signal—part 1: fundamentals, *Proceedings of the IEEE* 80 (4) (1992) 520–538.